

From Zero to Detail: Deconstructing Ultra-High-Definition Image Restoration from Progressive Spectral Perspective

Chen Zhao^{1*}, Zhizhou Chen^{1*}, Yunzhe Xu¹, Enxuan Gu², Jian Li³

Zili Yi¹, Qian Wang⁴, Jian Yang¹, Ying Tai^{1†}

¹Nanjing University, ²Dalian University of Technology, ³Tencent Youtu, ⁴China Mobile Institute

Abstract

Ultra-high-definition (UHD) image restoration faces significant challenges due to its high resolution, complex content, and intricate details. To cope with these challenges, we analyze the restoration process in depth through a progressive spectral perspective, and deconstruct the complex UHD restoration problem into three progressive stages: zero-frequency enhancement, low-frequency restoration, and high-frequency refinement. Building on this insight, we propose a novel framework, ERR, which comprises three collaborative sub-networks: the zero-frequency enhancer (ZFE), the low-frequency restorer (LFR), and the high-frequency refiner (HFR). Specifically, the ZFE integrates global priors to learn global mapping, while the LFR restores low-frequency information, emphasizing reconstruction of coarse-grained content. Finally, the HFR employs our designed frequency-windowed kolmogorov-arnold networks (FW-KAN) to refine textures and details, producing high-quality image restoration. Our approach significantly outperforms previous UHD methods across various tasks, with extensive ablation studies validating the effectiveness of each component. The code is available at [here](#).

1. Introduction

Ultra-high-definition (UHD) imaging has advanced rapidly, and has gained widespread attention across diverse areas [9, 21, 22, 39, 40, 69, 86]. However, UHD images captured under adverse conditions, such as low light, rain, or haze, often suffer from severe degradation [49]. The purpose of this paper is to explore UHD image restoration (IR).

With the remarkable success of deep learning [4, 11, 18, 20, 29, 30, 44–47, 54, 61, 73–76, 82, 84, 89, 91], a wide range of learning-based methods have been proposed to address IR challenges, focusing on convolutional neural networks (CNNs) and Transformer [2, 5, 24, 41, 43, 53, 70, 72, 79, 94]. Current state-of-the-art (SOTA) methods primarily enhance network performance by introducing more complex architectures [3, 23, 35, 37, 59, 65, 71, 77, 88].

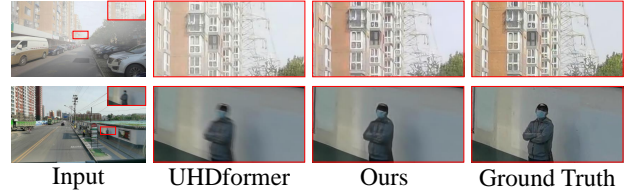


Figure 1. Visual comparison with the latest SOTA method.

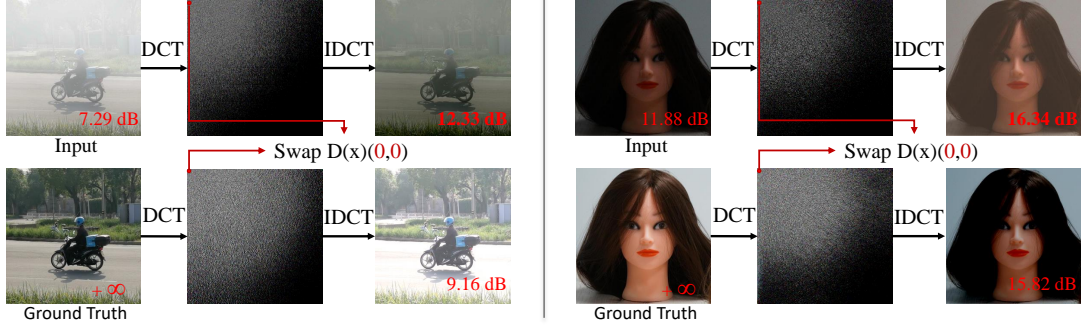
However, due to the ultra-high resolution and pixel density of UHD images, these advanced methods struggle to perform effectively in UHD scenarios.

Recently, several methods tailored for UHD IR have emerged [49, 51, 52, 60, 67, 95]. LLformer [52] achieved impressive performance by leveraging Transformers. However, due to the high computational cost, this approach cannot efficiently perform full-resolution inference on edge devices. UHDfour [21] reduced the resolution through 8× downsampling, enabling full-resolution inference of UHD images on edge devices. UHDformer [49] proposed a correction transformer that leverages high-resolution feature to guide the low-resolution restoration. Despite these methods relying on downsampling reduced computational costs, this *downsampling-enhancement-upsampling learning paradigm* inevitably leads to the loss of critical information [68]. Furthermore, the complexity of UHD images, characterized by *ultra-high resolution, substantial content, and intricate structural details*, poses significant challenges for restoration, making it difficult for existing methods to achieve efficient and high-quality results [68].

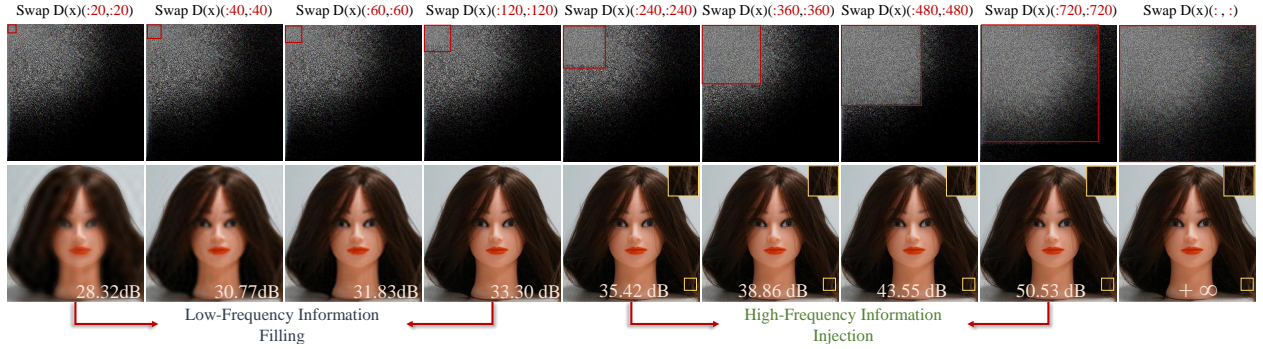
To investigate the issue of UHD IR in depth, we adopt a progressive frequency decoupling to examine the significance of various frequency components in restoration process. Initially, we map the degraded image (input) and the corresponding ground truth (GT) into the frequency domain using discrete cosine transform (DCT), exchanging the frequency information at the (0,0) position, known as the *zero frequency component*¹. We then reconstruct the exchanged frequency spectrum back into the spatial domain using inverse discrete cosine transform (IDCT), as illustrated in

*Equal contributions. † indicates corresponding author.

¹stanford.edu/signals.pdf



(a) We exchange the information at the (0,0) position in the DCT spectrum, which represents the global information.



(b) The low-frequency filling restores the coarse-grained content, while the high-frequency injection refines the fine-grained textures.

Figure 2. Our core motivation. Based on the observations in (a) and (b), we deconstruct the complex UHD restoration problem into three progressive stages: zero-frequency enhancement, low-frequency restoration, and high-frequency refinement.

Figure 2a. The zero-frequency component represents the direct-current information, reflecting the global and average characteristics of the image. We observe that the visual properties of the exchanged input and GT also swaps, and the PSNR value of the exchanged input slightly higher than that of the exchanged GT. This suggests that even if perfect non-zero frequency component is learned (e.g., the exchanged GT), acceptable results cannot be achieved, further indicating that *the zero-frequency component plays a crucial role in the early stages of restoration*. We progressively expand the range of exchanged frequency components and observe that as low-frequency component is filled, the structures and content are restored, while the injection of high-frequency information refines the details and textures, as shown in Figure 2b. *Based on the observation, we deconstruct the complex UHD IR problem into three progressive stages: zero-frequency enhancement, low-frequency restoration, and high-frequency refinement, each targeting to learn the global mapping, coarse-grained content, and fine-grained textures, respectively, thereby enhancing the quality of images*, as depicted in Figure 1.

Building on the insight, we develop a novel framework, termed ERR, which leverages progressive frequency decoupling to navigate the complexities of UHD images. ERR consists of three collaborative sub-networks: the zero-frequency enhancer (ZFE), the low-frequency restorer (LFR), and the high-frequency refiner (HFR). Specifically,

by incorporating global prior, the ZFE focuses on enhancing global information. The purpose of the LFR is to further restore the low-frequency information, emphasizing the reconstruction of the primary content. Finally, the HFR employs our meticulously designed frequency windowed kolmogorov-arnold networks (FW-KAN) to refine details and textures, achieving high-quality image restoration. Comparative results across multiple tasks indicate that our developed ERR achieves significant superiority over previous UHD methods. Furthermore, extensive ablation studies prove the effectiveness of our contributions.

In summary, the key contributions of our work are as follows:

- We conduct an in-depth analysis of UHD restoration from a progressive spectral perspective, deconstructing the complex UHD restoration problem into three progressive stages: zero-frequency enhancement, low-frequency restoration, and high-frequency refinement.
- Building on this insight, we propose a novel framework, termed **ERR**, which consists of three sub-networks: the zero-frequency enhancer (ZFE), the low-frequency restorer (LFR), and the high-frequency refiner (HFR).
- For the ZFE, we design a global perception transformer block (GPTB) to more effectively capture global representations. For the HFR, we develop a frequency-windowed KAN (FW-KAN) to refine fine-grained information, thereby enhancing image details and textures.

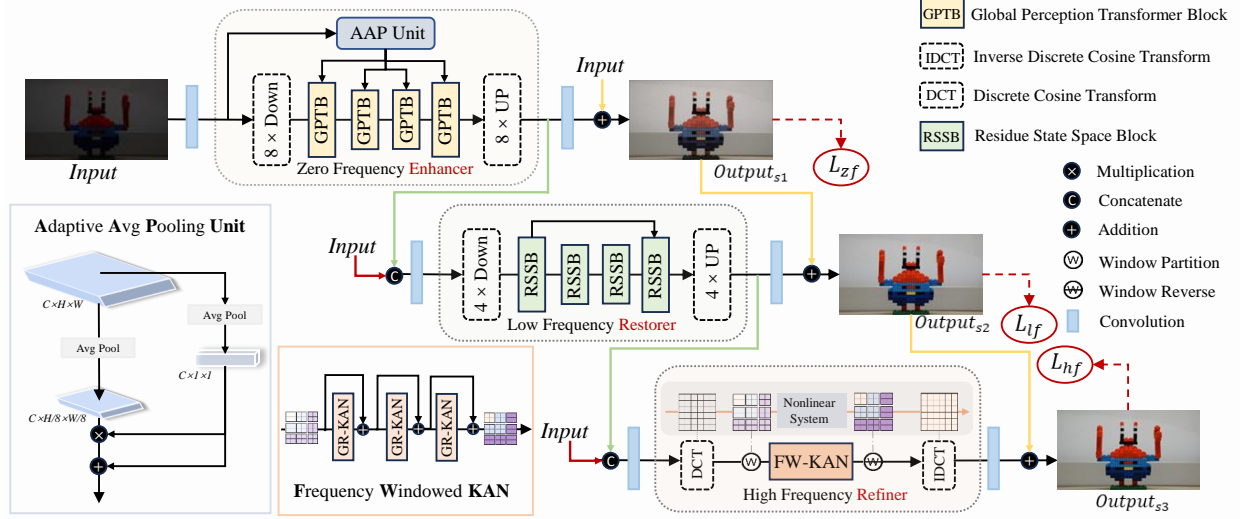


Figure 3. Overall framework of our proposed ERR. Building on the insight from progressive spectral perspective, ERR consists of three collaborative sub-networks: the zero-frequency enhancer (ZFE), the low-frequency restorer (LFR), and the high-frequency refiner (HFR).

2. Related Works

2.1. Ultra-high-definition Image Restoration

As UHD imaging becomes more pervasive, the field of UHD restoration is drawing heightened attention [9, 22, 49, 52, 57, 69, 86, 87, 95]. Zheng et al. [86] introduced a multi-guided bilateral upsampling model for UHD dehazing. UHDFour [21] downsampled UHD images by a factor of 8, enabling full-resolution inference on edge devices. UHD-former [49] leverages high-resolution information to guide the low-resolution restoration. UDR-Mixer [1] facilitated low-resolution spatial feature restoration through frequency feature modulation. These methods [1, 21, 49, 86] share a similar paradigm: learning from downsampled images to ease computational demands. However, this *downsampling-enhancement-upsampling paradigm* inevitably results in the loss of essential information [68]. Moreover, the complexity of UHD images—with *ultra-high resolution, rich content, and complex structures*—poses major challenges for restoration, making it difficult for existing methods to achieve both efficiency and high quality [68].

2.2. Frequency Learning

An increasing number of studies [7, 12, 27, 28, 31–34, 36, 81, 83, 90, 93, 95] leverage frequency domain characteristics across various tasks. DSGAN [12] separated the low and high image frequencies via the low- and high-pass filters. LaMa [42] uses the frequency convolution for image inpainting. DeepRFT [33] proposed a simple res-fft-relu-block for image deblurring. Fourmer [92] leverages the Fourier transform to model global dependencies for image restoration. To exploit the characteristics of different frequency signals, recent works [16, 17, 80, 95] have explored

discrete wavelet transform (DWT) to achieve decoupling purposes for IR tasks. Unlike previous frequency-domain approaches, we deconstruct the complex UHD restoration problem into three stages from a progressive frequency perspective, focusing on learning the global mapping, coarse-grained content, and fine-grained textures, respectively.

3. Methodology

3.1. Overall Framework

Given a UHD degraded image as input, we aim to learn a network to generate a UHD output that eliminates the degradation. The framework of ERR is shown in Figure 3, which integrates three collaborative sub-networks: the zero-frequency enhancer (ZFE), the low-frequency restorer (LFR), and the high-frequency refiner (HFR). Specifically, ZFE learns global representations within low-resolution space. To efficiently learn content representations, the LFR restores low-frequency information of the degraded UHD image within mid-resolution space. In the final stage, the HFR employs our designed frequency windowed kolmogorov-arnold networks (FW-KAN) to refine fine-grained information within full-resolution space, enhancing image details and textures to further achieve high-quality image reconstruction.

3.2. Discrete Cosine Transform

Frequency decoupling and analysis have been widely applied across various fields. We primarily use the discrete cosine transform (DCT) to analyze and deconstruct UHD images. Given an input $x \in \mathbb{R}^{H \times W \times C}$, whose spatial shape is $H \times W$, the DCT transform \mathcal{D} which converts the input

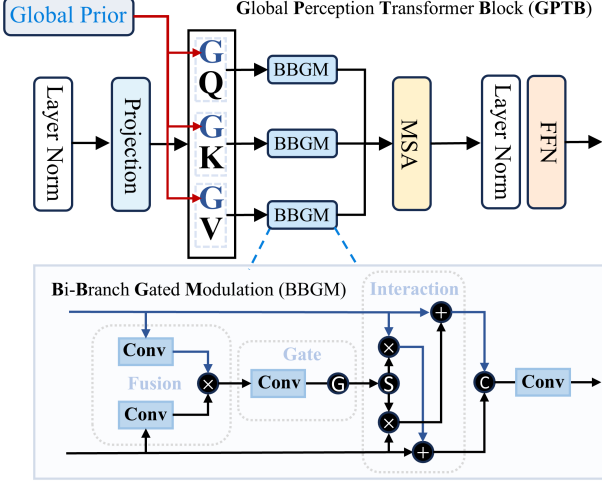


Figure 4. The architecture of the Global Perception Transformer Block (GPTB).

I to the frequency space F can be expressed as:

$$\begin{aligned} \mathcal{D}(x)(u, v) &= F(u, v) \\ &= \sum_{h=0}^{H-1} \sum_{w=0}^{W-1} x(h, w) \cdot \cos \frac{(2h+1)u\pi}{2W} \cdot \cos \frac{(2w+1)v\pi}{2H}, \end{aligned} \quad (1)$$

where h, w and u, v stand for the coordinates in the RGB color space and in the frequency space. \mathcal{D}^{-1} denotes the inverse discrete cosine transform (IDCT).

The core motivation. To cope with the complexities of UHD images, we analyze and explore from progressive frequency decoupling perspective. Figure 2 illustrates our motivations schematically. Firstly, we investigate the importance of the zero-frequency component, which can be represented as $\mathcal{D}(x)(0, 0)$. The zero-frequency component refers to the direct-current information, reflecting the global and average characteristics of the image. We exchange the zero-frequency components between the degraded image (input) and the GT, obtaining the exchanged input and GT. The exchanged input retains a perfect zero-frequency component while containing degraded non-zero frequency elements, while the exchanged GT is its inverse. As shown in the two cases in Figure 2a, the quality of the exchanged input is significantly higher than that of the exchanged GT. Therefore, even if perfect non-zero frequency components can be learned (e.g., the exchanged GT), satisfactory results cannot be achieved. This observation suggests that *in the early stages of restoration, a stronger focus should be placed on learning the zero-frequency component, i.e., capturing the global mapping*. We sequentially expand the range of frequency components, exchanging the first k levels, which can be expressed as $\mathcal{D}(x)(:k, :k)$. It is evident that we can observe two trends in the changes of image quality. As the low-frequency information is progressively filled, the content and structural information of the coarse-grained level are gradually restored, while the injection of

high-frequency information refines the details and textures of the fine-grained level. The PSNR value and visual quality of the input gradually improve, as illustrated in Figure 2b. This step-by-step process from zero to detail implies a gradual enhancement in image quality; in contrast, the reverse process fails to achieve high-quality results.

Based on this observation and analysis, our goal is to deconstruct the complex UHD restoration problem into three progressive stages: *zero-frequency enhancement, low-frequency restoration, and high-frequency refinement, each focusing on learning the global mapping, coarse-grained content, and fine-grained textures, respectively*.

3.3. Zero Frequency Enhancer

ZFE aims to learn global mapping within low-resolution space, primarily through two core modules: the adaptive average pooling (AAP) unit and the global perception transformer block (GPTB). The purpose of the AAP unit is to extract global prior within the full-resolution space. By leveraging the captured global prior, the GPTB can more effectively enhance global representation learning.

AAP unit. The zero-frequency component represents the direct current (DC) information, which reflects the global and average characteristics of the UHD image. Consequently, we employ average pooling (AvP) in the full-resolution space to capture global prior. Given an input feature map $x \in \mathbb{R}^{H \times W \times C}$, we aim to extract global features while preserving local characteristics. To achieve the target, we employ a combination of global AvP and local AvP. The AAP unit can be expressed mathematically as:

$$G = \mathcal{AAP}(x) = AvP_{1,1}(x) \odot AvP_{\frac{H}{8}, \frac{W}{8}}(x) + AvP_{1,1}(x), \quad (2)$$

where $AvP_{1,1}$ represents the global AvP with a pooling size of $(1, 1)$, and $AvP_{\frac{H}{8}, \frac{W}{8}}(x)$ denotes the local AvP with a pooling size of $(\frac{H}{8}, \frac{W}{8})$. Moreover, to enhance feature representation capacity, we introduce multi-scale learning within our AAP unit. \odot indicates the element-wise multiplication. $G \in \mathbb{R}^{\frac{H}{8} \times \frac{W}{8} \times C}$ refers to the global prior.

GPTB. The low-resolution features $x_{\text{low}} \in \mathbb{R}^{\frac{H}{8} \times \frac{W}{8} \times C}$ are obtained from an input x via 8x downsampling. Then, $x_{\text{low}} \in \mathbb{R}^{\frac{H}{8} \times \frac{W}{8} \times C}$ is sent to several GPTB to learn the global mapping. Figure 4 shows the detail architecture of GPTB, where bi-branch gated modulation (BBGM) is designed to integrate low-resolution features with global priors. The computation can be denoted in the GPTB as:

$$Q, K, V = \mathcal{S}(\text{Projection}(\text{LN}(x_{\text{low}}^{i-1}))), \quad (3)$$

$$\hat{Q}, \hat{K}, \hat{V} = \mathcal{B}(G, Q), \mathcal{B}(G, K), \mathcal{B}(G, V), \quad (4)$$

$$\hat{x} = \text{MSA}(\hat{Q}, \hat{K}, \hat{V}) + x_{\text{low}}^{i-1}, \quad (5)$$

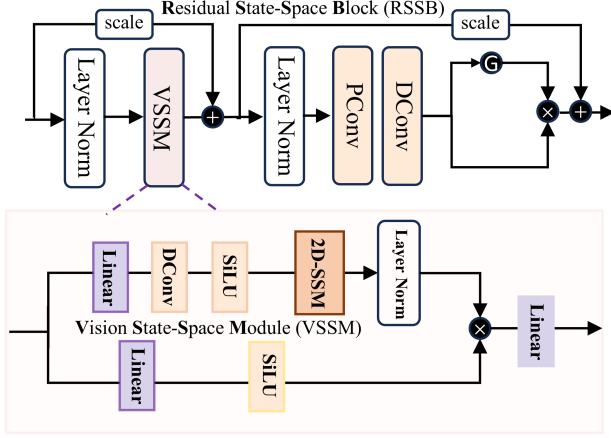


Figure 5. The architecture of the residue state space block (RSSB).

$$x_{\text{low}}^i = \text{FFN}(\text{LN}(\hat{x})) + \hat{x}, \quad (6)$$

where LN, MSA, and \mathcal{S} refer to layer normalization, multi-head self-attention, and split operation, respectively. x_{low}^{i-1} represents the input embeddings of the current GPTB. The BBGM \mathcal{B} comprises three part—fusion, gating, and interaction—that collectively ensure a comprehensive integration of features. The BBGM can be expressed as follows:

$$W_a, W_b = \mathcal{S}(\delta(\text{Conv}(\text{Conv}(G) \odot \text{Conv}(F)))), \quad (7)$$

$$\hat{F} = \mathcal{C}[F + W_a \odot G, G + W_a \odot F], \quad (8)$$

where F and \hat{F} represent the original embedding and the features fused with the global prior G . \mathcal{C} and δ refer to concat operation and Gelu function.

Regularization. In the first stage, we primarily constrain the zero-frequency component of the generated image, focusing on learning global representation. Given that the output of the first stage is O_{s1} , zero-frequency regularization \mathcal{L}_{zf} can be mathematically expressed as:

$$\mathcal{L}_{zf} = \|\mathcal{D}(O_{s1})(0, 0) - \mathcal{D}(GT)(0, 0)\|_1. \quad (9)$$

3.4. Low Frequency Restorer

To efficiently learn content representations, the LFR restores low-frequency information within mid-resolution space. The mid-resolution features $x_{\text{mid}} \in \mathbb{R}^{\frac{H}{4} \times \frac{W}{4} \times C}$ are captured via 4x downsampling. The core operator of the LFR is the residue state space block (RSSB), also known as the Mamba block [10, 13, 15], effectively capturing long-range dependencies and global features with low computational cost. The detailed structure of the RSSB is illustrated in Figure 5. The RSSB can be mathematically expressed as:

$$x' = \text{VSSM}(\text{LN}(x_{\text{mid}}^{i-1})) + s \cdot x_{\text{mid}}^{i-1}, \quad (10)$$

$$x_{\text{mid}}^i = \text{PC}(\delta_g(\text{DC}(\text{PC}(\text{LN}(x'))))) + s' \cdot x', \quad (11)$$

Table 1. Linear system means UHDformer without all non-linear functions. The difference on UHD-LL [21] suggests that the non-linear functions mainly injects high-frequency information.

Method	Linear system		UHDformer		Difference	
	Low	High	Low	High	Low	High
PSNR \uparrow	28.70	34.68	27.92	36.82	-0.78	2.14
SSIM \uparrow	0.9873	0.8539	0.9820	0.9081	-0.0053	0.0542

where PC and DC represent point-wise and depth-wise convolution, respectively. δ_g is the function of non-linear gate, similar to SimpleGate, dividing the input along the channel dimension into two features $\mathbf{F}_1, \mathbf{F}_2 \in \mathbb{R}^{H \times W \times \frac{C}{2}}$. The output is then calculated by $\delta_g(F) = \delta(\mathbf{F}_1) \cdot \mathbf{F}_2$. The detailed description of the vision state-space module (VSSM) [13] can be found in the supplementary materials. **Regularization.** In this stage, our objective is to learn the low-frequency components, with a primary focus on the restoration of coarse-grained structures and content. Given that the output of this stage is O_{s2} and frequency cutoff k is hyper parameter, low-frequency regularization \mathcal{L}_{lf} can be mathematically expressed as:

$$\mathcal{L}_{lf} = \sum_{i=0}^k \sum_{j=0}^k \|\mathcal{D}(O_{s2})(i, j) - \mathcal{D}(GT)(i, j)\|_1, \quad (12)$$

where $(i, j) \neq (0, 0)$.

3.5. High Frequency Refiner

In the final stage, the HFR employs the designed FW-KAN to refine image details and textures within full-resolution space, further achieving high-quality image reconstruction.

The motivation for KAN. Existing study [8] on explainability in deep learning introduces an intriguing perspective: the linear system acts as a low-frequency learner, while *the non-linear system injects high-frequency information*. Inspired by this, we further investigate this behavior in UHDformer by removing all non-linear activation functions. Table 1 validates that the non-linear function primarily injects high-frequency information. Recently, KAN [25] has become well-known as a learnable non-linear operator with powerful non-linear expression capabilities, which motivates us to explore it as the core operator in our final stage.

FW-KAN. Group-rational KAN (GR-KAN) [64] addresses the high complexity and optimization challenges of the original KAN [25] by introducing rational activation functions and variance-preserving initialization. However, applying GR-KAN in the UHD original resolution space continues to require substantial memory. Additionally, due to the pixel density of UHD images, high-frequency details become exceedingly complex. To alleviate these issues, we adopt a window partition (WP) in the DCT spectrum to partition high- and low-frequency information into blocks, which not only reduces memory consumption but also encourages the model to concentrate more effectively on high-frequency detail learning, as illustrated in the detailed FW-

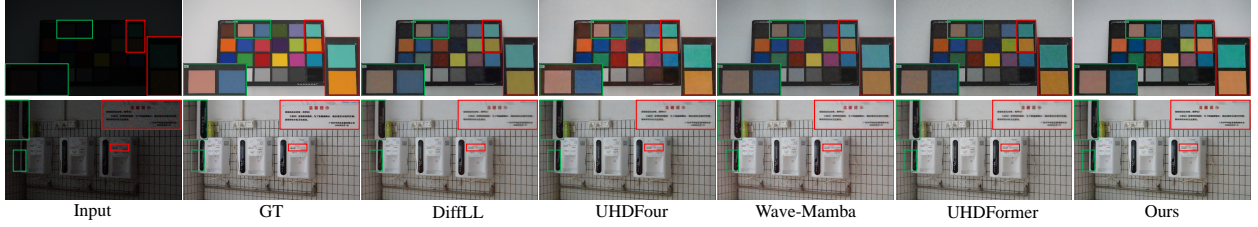


Figure 6. Visual comparison with other SOTA methods on the UHD-LL [21].

KAN diagram in Figure 3. FW-KAN consists of multiple stacked GR-KAN. Given the original resolution feature $x_{high} \in \mathbb{R}^{H \times W \times C}$, HFR can be expressed as:

$$x' = \mathcal{D}^{-1}(\text{WR}(\text{FW-KAN}(\text{WP}(\mathcal{D}(x_{high}))))), \quad (13)$$

where \mathcal{D}^{-1} and WR stand for inverse DCT and window reverse operation.

Regularization. In the final stage, our objective is to inject high-frequency information, with an emphasis on the refinement of fine-grained texture and details. Given that the output of this stage is O_{s3} , high-frequency regularization \mathcal{L}_{lf} can be mathematically expressed as:

$$\mathcal{L}_{hf} = \sum_{i=0}^N \sum_{j=0}^N \|\mathcal{D}(O_{s3})(i, j) - \mathcal{D}(GT)(i, j)\|_1, \quad (14)$$

where $(i \geq k) \vee (j \geq k)$,

where N denotes the maximum horizontal and vertical index of the spectrum, and k represents the frequency cutoff.

3.6. Loss

At any stage l , we employ L1 and SSIM loss, and the reconstruction loss \mathcal{L}_{rec} can be expressed as:

$$\mathcal{L}_{rec} = \sum_{l=1}^3 [\mathcal{L}_1(O_l, GT) + \mathcal{L}_{ssim}(O_l, GT)], \quad (15)$$

where O_l represents the output at stage l . The total loss function \mathcal{L}_{total} can be defined as:

$$\mathcal{L}_{total} = \mathcal{L}_{rec} + \mathcal{L}_{zf} + \mathcal{L}_{lf} + \mathcal{L}_{hf}. \quad (16)$$

4. Experiments

In this section, we evaluate our approach in comparison to SOTA methods across four public UHD image restoration benchmarks: enhancement of low-light images, removal of rain artifacts, image deblurring, and haze reduction.

4.1. Experimental Settings

Implementation details. All experiments are conducted on a NVIDIA A6000 GPU. We train the models using the AdamW optimizer with an initial learning rate of 0.0005, which is gradually reduced to $1e-7$ after 100k iterations using cosine annealing [26]. The patch size is set to 512×512 , with a batch size of 6.

Table 2. Comparison of quantitative results on UHD-LL [21].

Methods	PSNR \uparrow	SSIM \uparrow	LPIPS \downarrow	Parameter \downarrow
IFT [85]	21.96	0.870	0.324	11.56M
SNR-Aware [62]	22.72	0.877	0.304	40.08M
Uformer [56]	19.28	0.849	0.356	20.62M
Restormer [70]	22.25	0.871	0.289	26.11M
DiffLL [16]	21.36	0.872	0.239	17.29M
LLFormer [52]	22.79	0.853	0.264	13.15M
UHDFour [21]	26.22	0.900	0.239	17.54M
Wave-Mamba [95]	<u>27.35</u>	0.913	0.185	1.258M
UHDFormer [49]	27.11	<u>0.927</u>	0.245	0.339M
Ours _{stage1}	24.61	0.841	0.455	-
Ours _{stage2}	27.33	0.925	0.226	-
Ours	27.57	0.932	<u>0.214</u>	<u>1.131M</u>

Table 3. Comparison of quantitative results on 4K-Rain13k [1].

Methods	PSNR \uparrow	SSIM \uparrow	LPIPS \downarrow	Parameter \downarrow
JORDER-E [63]	30.46	0.912	0.209	4.21M
RCDNet [50]	30.83	0.921	0.196	3.17M
SPDNet [66]	31.81	0.922	0.195	<u>3.04M</u>
IDT [58]	32.91	0.948	0.124	16.41M
Restormer [70]	33.02	0.933	0.173	26.12M
DRSformer [2]	32.94	0.933	0.171	33.65M
UDR-S2Former [2]	33.36	0.946	<u>0.122</u>	8.53M
UDR-Mixer [1]	34.28	<u>0.951</u>	0.133	4.90M
Ours _{stage1}	27.13	0.827	0.350	-
Ours _{stage2}	34.21	0.943	0.131	-
Ours	34.48	0.952	0.120	1.131M

Datasets. We evaluate our method on four UHD restoration benchmarks. For low-light enhancement, we conduct experiments using the UHD-LL dataset [21]. The image de-raining performance is assessed on the 4K-Rain13k dataset [1]. For the tasks of image dehazing and deblurring, we utilize the UHD-Haze [49] and UHD-Blur [49] datasets.

Evaluation. We mainly adopt peak signal to noise ratio (PSNR) [14] and structural similarity (SSIM) [55] to evaluate the performance of networks. Additionally, LPIPS [78] are utilized to evaluate perceptual performance. For methods incapable of full-resolution inference, following [21], we adopted a splitting strategy.

4.2. Comparisons with State-of-the-Art Methods

Low-light image enhancement. We trained the proposed ERR model on the UHD-LL dataset and compared it against state-of-the-art low-light enhancement methods, including IFT [85], SNR-Aware [62], Uformer [56], Restormer [70], DiffLL [16], LLFormer [52], UHDFour [21], UHDFormer [49], and Wave-Mamba [95]. The quantitative results in Table 2 demonstrate that our ERR significantly enhances

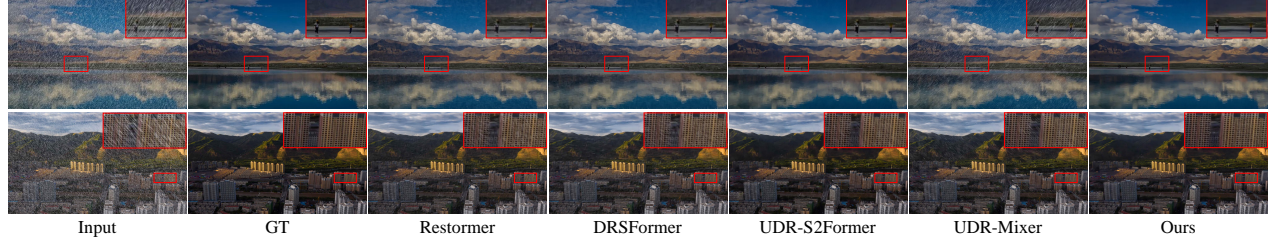


Figure 7. Visual comparison with other SOTA methods on the 4K-Rain13k [1].

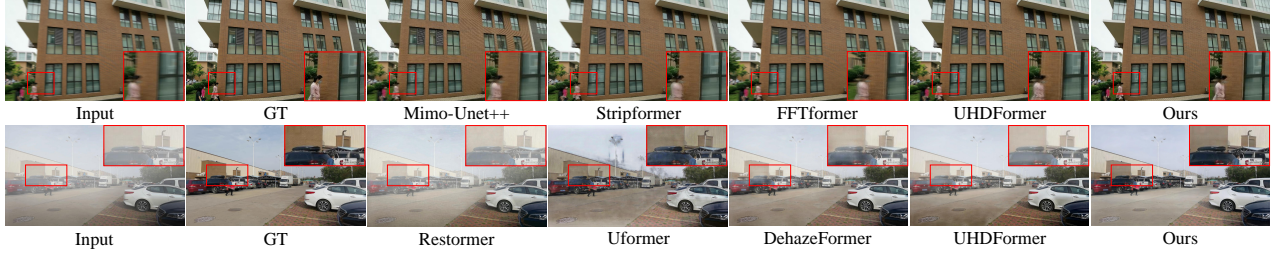


Figure 8. Visual comparison with other SOTA methods on the UHD-Haze and UHD-Blur [49].

Table 4. Comparison of quantitative results on UHD-Haze [49].

Methods	PSNR \uparrow	SSIM \uparrow	Parameter \downarrow
UHD [86]	18.04	0.811	34.5M
Restormer [70]	12.72	0.693	26.1M
Uformer [56]	19.83	0.737	20.6M
DehazeFormer [38]	15.37	0.725	2.5M
UHDFormer [49]	22.59	0.943	0.339M
Ours _{stage1}	16.15	0.621	-
Ours _{stage2}	24.67	0.923	-
Ours	25.12	0.950	1.131M

performance, improving PSNR and SSIM metrics and surpassing all baselines. Figure 6 further provides visual evaluations on the UHD-LL dataset, where our ERR preserves finer details and achieves superior perceptual quality.

Image deraining. We evaluate the effectiveness of UHD deraining on the 4K-Rain13k, comparing our ERR with recent methods, including JORDER-E [63], RCDNet [50], SPDNet [66], IDT [58], Restormer [70], UDR-S2Former [2], and UDR-Mixer [1]. Quantitative results in Table 3 demonstrate that our method achieves the highest scores across all metrics, while reducing model parameters. The visual results in Figure 7 show that our method effectively removes rain streaks while preserving rich texture details.

Image dehazing. Table 4 summarizes the quantitative results on the UHD-Haze, comparing our method with recent advanced methods such as UHD [86], Restormer [70], Uformer [56], DehazeFormer [38], and UHDFormer [49]. Our model achieves a PSNR improvement of 2.53dB with a relatively small number of parameters, and attains the highest SSIM score. Qualitative results in Figure 8 further demonstrate that ERR effectively restores clear images, whereas other methods struggle to fully remove dense haze.

Image deblurring. We evaluate the deblurring performance of our model on the UHD-Blur dataset, comparing it with recent methods including MIMO-UNet++ [6], Restormer [70], Uformer [56], Stripformer [48], FFTformer [19], and UHDFormer [49]. As shown in Table 5, our

Table 5. Comparison of quantitative results on UHD-Blur [49].

Methods	PSNR \uparrow	SSIM \uparrow	Parameter \downarrow
MIMO-Unet++ [6]	25.03	0.811	16.1M
Restormer [70]	25.21	0.693	26.1M
Uformer [56]	25.27	0.737	20.6M
Stripformer [48]	25.05	0.725	19.7M
FFTformer [19]	25.41	0.725	16.6M
UHDFormer	28.82	0.844	0.339M
Ours _{stage1}	24.16	0.705	-
Ours _{stage2}	29.68	0.857	-
Ours	29.72	0.861	1.131M

Table 6. Effect of different frequency cutoffs k .

The value of k	32	64	96	128	256
PSNR \uparrow	26.71	27.57	27.52	27.29	27.25
SSIM \uparrow	0.9296	0.9326	0.9323	0.9319	0.9313

approach achieves the highest PSNR and SSIM scores, demonstrating its superior effectiveness. Qualitative results in Figure 8 further reveal that ERR generates clearer details.

4.3. Ablation Study

We perform comprehensive ablation experiments to verify the effectiveness of each contribution and design. All ablations are conducted on UHD-LL [21].

Effect of different frequency cutoffs k . The ablation results with different cutoffs k are shown in Table 6, which indicate that both excessively large and small values of k negatively affect performance. A small k overcomplicates high-frequency component, increasing the learning difficulty of the HFR, while a large k introduces excessive low-frequency component, hindering the restoration of the LFR.

Ablation with different architecture. Table 7 demonstrates the impact of all components on our framework. A, B, and C validate the effectiveness of our frequency regularizations, while D, E, and F confirm the efficacy of each stage’s network. The superior performance of D, E, and F over A, B, and C suggests that, without the frequency constraints, the networks face challenges in optimization. H outperforms G, indicating that the progressive residual is

Table 7. Ablation study with different architecture. PR refers to progressive residual, as indicated by the yellow arrows between each stage in Figure 3.

Method	\mathcal{L}_{zf}	\mathcal{L}_{lf}	\mathcal{L}_{hf}	ZFE	LFR	HFR	PR	PSNR \uparrow	SSIM \uparrow
A	×	✓	✓	✓	✓	✓	✓	26.73	0.9286
B	✓	×	✓	✓	✓	✓	✓	26.57	0.9277
C	✓	✓	×	✓	✓	✓	✓	26.80	0.9290
D	×	✓	✓	×	✓	✓	✓	27.01	0.9311
E	✓	×	✓	✓	×	✓	✓	26.81	0.9186
F	✓	✓	×	✓	✓	×	✓	27.04	0.9266
G	✓	✓	✓	✓	✓	✓	×	26.99	0.9307
H	✓	✓	✓	✓	✓	✓	✓	27.57	0.9326

Table 8. Ablation study with the detail design of the ZFE.

AAP		BBGM			Metrics	
$AvP_{1,1}$	$AvP_{\frac{H}{8}, \frac{W}{8}}(x)$	Fusion	Gate	Interaction	PSNR \uparrow	SSIM \uparrow
×	×	×	×	×	26.70	0.9289
×	✓	✓	✓	✓	27.16	0.9315
✓	×	✓	✓	✓	27.18	0.9316
✓	✓	×	✓	✓	26.00	0.9251
✓	✓	✓	×	✓	26.20	0.9268
✓	✓	✓	✓	×	26.04	0.9256
✓	✓	✓	✓	✓	27.57	0.9326

Table 9. Ablation study with the detail design of the HFR.

Model	w/o DCT	w/o WP	w/o WP & DCT	Full Model
PSNR \uparrow	26.88	26.97	25.78	27.57
SSIM \uparrow	0.9308	0.9296	0.9247	0.9326

more effective than using the input at each stage.

Ablation with the detail design of the ZFE. In Table 8, we discuss the details of the ZFE, focusing on the AAP unit for global prior generation and the BBGM for global prior integration. First, we remove the entire AAP unit, as well as the global and local AvP separately, and this results confirm the effectiveness of our prior design. Next, removing each module in the BBGM leads to poorer performance, indicating the critical role of prior integration strategy for model performance. Figure 9 illustrates visual ablation results for the zero-frequency part.

Ablation with the detail design of the HFR. Table 9 validates the effectiveness of DCT and WR operations in HFR. The models without DCT or WR achieve lower performance, suggesting that window partitioning in the DCT spectrum enhances the model’s ability to capture high-frequency information more effectively. The model without WP & DCT (W & D) achieves the lowest performance, indicating that WP and DCT alone are effective in improving performance. Figure 10 illustrates visual ablation results for the high-frequency part, where our method achieves the best visual results in terms of details and textures.

Ablation for FW-KAN. In Table 10, we compare our FW-KAN with other nonlinear operators, specifically MLP and the original KAN. For MLP, we employ a two-layer activa-

Table 10. Ablation for FW-KAN.

Model	MLP-6	MLP-12	MLP-24	KAN	FW-KAN
PSNR \uparrow	26.03	26.58	26.97	20.48	27.57
SSIM \uparrow	0.9294	0.9297	0.9311	0.8836	0.9326
Parameter \downarrow	30.73K	35.63K	45.42K	27.57K	27.47K

Table 11. Comparison of inference time on 4K images.

Model	LLformer	UHDformer	Wave-Mamba	Ours
Inference time (s) \downarrow	41.056	0.887	0.618	0.532



Figure 9. Visual ablation results for the zero-frequency part.

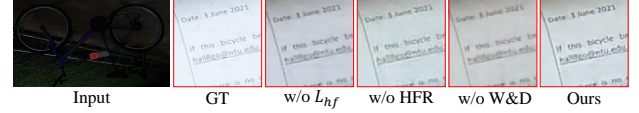


Figure 10. Visual ablation results for the high-frequency part.



Figure 11. Limitations in extremely low-light scenarios.

tion structure, defined as linear-ReLU-linear-ReLU-linear, to enhance nonlinear expressiveness. MLP-6, MLP-12, and MLP-24 refer to MLPs with 6, 12, and 24 layers. Experiments show that, compared to MLP, our FW-KAN can learn complex representations with fewer parameters, while the original KAN encounters optimization challenges.

Inference efficiency. Table 11 presents a comparison of inference times between our method and baselines. LLFormer, which cannot perform full-resolution inference, incurs a high time cost. Our approach demonstrates the fastest inference efficiency among recent UHD methods.

5. Conclusion

In the paper, we develop a novel framework, namely ERR, which comprises three sub-networks: the ZFE to capture global information, the LFR to reconstruct primary content, and the HFR for detail refinement. ERR shows SOTA performance on multiple UHD tasks, and extensive ablation experiments prove that each component is effective.

Limitations and future works. Although our method achieves outstanding performance, it remains challenging to achieve satisfactory results in extreme scenarios, as shown in Figure 11. Therefore, mitigating this weakness will be the focus of our future research.

Acknowledgments. This work was supported by Natural Science Foundation of China: No. 62406135, Natural Science Foundation of Jiangsu Province: BK20241198, Gusu Innovation and Entrepreneur Leading Talents: No. ZX2024362 and Nanjing University-China Mobile Communications Group Co. Ltd. Joint Institute.

References

- [1] Hongming Chen, Xiang Chen, Chen Wu, Zhuoran Zheng, Jinshan Pan, and Xianping Fu. Towards ultra-high-definition image deraining: A benchmark and an efficient method. *arXiv preprint arXiv:2405.17074*, 2024. 3, 6, 7
- [2] Xiang Chen, Hao Li, Mingqiang Li, and Jinshan Pan. Learning a sparse transformer network for effective image deraining. In *Proceedings of the IEEE/CVF Conference on Computer Vision and Pattern Recognition*, pages 5896–5905, 2023. 1, 6, 7
- [3] Xiang Chen, Jinshan Pan, and Jiangxin Dong. Bidirectional multi-scale implicit neural representations for image deraining. In *Proceedings of the IEEE/CVF Conference on Computer Vision and Pattern Recognition*, pages 25627–25636, 2024. 1
- [4] Zhenan Chen, Yajie Li, Haofan Wang, Zhibo Chen, Zhengkai Jiang, Jun Li, Qian Wang, Jian Yang, and Ying Tai. Region-aware text-to-image generation via hard binding and soft refinement. *CoRR*, abs/2411.06558, 2024. 1
- [5] Senlin Cheng and Haopeng Sun. Spt: Sequence prompt transformer for interactive image segmentation. *arXiv preprint arXiv:2412.10224*, 2024. 1
- [6] Sung-Jin Cho, Seo-Won Ji, Jun-Pyo Hong, Seung-Won Jung, and Sung-Jea Ko. Rethinking coarse-to-fine approach in single image deblurring. In *Proceedings of the IEEE/CVF international conference on computer vision*, pages 4641–4650, 2021. 7
- [7] Yuning Cui, Wenqi Ren, Xiaochun Cao, and Alois Knoll. Image restoration via frequency selection. *IEEE Transactions on Pattern Analysis and Machine Intelligence*, 2023. 3
- [8] Haoyu Deng, Zijing Xu, Yule Duan, Xiao Wu, Wenjie Shu, and Liang-Jian Deng. Exploring the low-pass filtering behavior in image super-resolution. *arXiv preprint arXiv:2405.07919*, 2024. 5
- [9] Senyou Deng, Wenqi Ren, Yanyang Yan, Tao Wang, Fenglong Song, and Xiaochun Cao. Multi-scale separable network for ultra-high-definition video deblurring. In *Proceedings of the IEEE/CVF International Conference on Computer Vision*, pages 14030–14039, 2021. 1, 3
- [10] Chenyu Dong, Chen Zhao, Weiling Cai, and Bo Yang. Omamba: O-shape state-space model for underwater image enhancement. *CoRR*, abs/2408.12816, 2024. 5
- [11] Ruicheng Feng, Chongyi Li, and Chen Change Loy. Kalman-inspired feature propagation for video face super-resolution. *CoRR*, abs/2408.05205, 2024. 1
- [12] Manuel Fritsche, Shuhang Gu, and Radu Timofte. Frequency separation for real-world super-resolution. In *2019 IEEE/CVF International Conference on Computer Vision Workshop (ICCVW)*, pages 3599–3608. IEEE, 2019. 3
- [13] Hang Guo, Jinmin Li, Tao Dai, Zhihao Ouyang, Xudong Ren, and Shu-Tao Xia. Mambair: A simple baseline for image restoration with state-space model. In *European Conference on Computer Vision*, pages 222–241. Springer, 2025. 5
- [14] Alain Hore and Djemel Ziou. Image quality metrics: Psnr vs. ssim. In *2010 20th international conference on pattern recognition*, pages 2366–2369. IEEE, 2010. 6
- [15] Xiantao Hu, Ying Tai, Xu Zhao, Chen Zhao, Zhenyu Zhang, Jun Li, Bineng Zhong, and Jian Yang. Exploiting multimodal spatial-temporal patterns for video object tracking. *CoRR*, abs/2412.15691, 2024. 5
- [16] Hai Jiang, Ao Luo, Haoqiang Fan, Songchen Han, and Shuaicheng Liu. Low-light image enhancement with wavelet-based diffusion models. *ACM Transactions on Graphics (TOG)*, 42(6):1–14, 2023. 3, 6
- [17] Kui Jiang, Wenxuan Liu, Zheng Wang, Xian Zhong, Junjun Jiang, and Chia-Wen Lin. Dawn: Direction-aware attention wavelet network for image deraining. In *Proceedings of the 31st ACM international conference on multimedia*, pages 7065–7074, 2023. 3
- [18] Yeying Jin, Xin Li, Jiadong Wang, Yan Zhang, and Malu Zhang. Raindrop clarity: A dual-focused dataset for day and night raindrop removal. In *Computer Vision - ECCV 2024 - 18th European Conference, Milan, Italy, September 29-October 4, 2024, Proceedings, Part VI*, pages 1–17. Springer, 2024. 1
- [19] Lingshun Kong, Jiangxin Dong, Jianjun Ge, Mingqiang Li, and Jinshan Pan. Efficient frequency domain-based transformers for high-quality image deblurring. In *Proceedings of the IEEE/CVF Conference on Computer Vision and Pattern Recognition*, pages 5886–5895, 2023. 7
- [20] Bingchen Li, Xin Li, Hanxin Zhu, Yeying Jin, Ruoyu Feng, Zhizheng Zhang, and Zhibo Chen. Sed: Semantic-aware discriminator for image super-resolution. In *IEEE/CVF Conference on Computer Vision and Pattern Recognition, CVPR 2024, Seattle, WA, USA, June 16-22, 2024*, pages 25784–25795. IEEE, 2024. 1
- [21] Chongyi Li, Chun-Le Guo, Man Zhou, Zhixin Liang, Shangchen Zhou, Ruicheng Feng, and Chen Change Loy. Embedding fourier for ultra-high-definition low-light image enhancement. *arXiv preprint arXiv:2302.11831*, 2023. 1, 3, 5, 6, 7
- [22] Quewei Li, Feichao Li, Jie Guo, and Yanwen Guo. Uhdnerf: Ultra-high-definition neural radiance fields. In *Proceedings of the IEEE/CVF International Conference on Computer Vision*, pages 23097–23108, 2023. 1, 3
- [23] Yawei Li, Yuchen Fan, Xiaoyu Xiang, Denis Demandolx, Rakesh Ranjan, Radu Timofte, and Luc Van Gool. Efficient and explicit modelling of image hierarchies for image restoration. In *Proceedings of the IEEE/CVF Conference on Computer Vision and Pattern Recognition*, pages 18278–18289, 2023. 1
- [24] Jingyun Liang, Jiezhang Cao, Guolei Sun, Kai Zhang, Luc Van Gool, and Radu Timofte. Swinir: Image restoration using swin transformer. In *Proceedings of the IEEE/CVF international conference on computer vision*, pages 1833–1844, 2021. 1
- [25] Ziming Liu, Yixuan Wang, Sachin Vaidya, Fabian Ruehle, James Halverson, Marin Soljačić, Thomas Y Hou, and Max Tegmark. Kan: Kolmogorov-arnold networks. *arXiv preprint arXiv:2404.19756*, 2024. 5
- [26] Ilya Loshchilov and Frank Hutter. Sgdr: Stochastic gradient descent with warm restarts. *arXiv preprint arXiv:1608.03983*, 2016. 6

- [27] Yiwei Lou, Dexuan Xu, Rongchao Zhang, Jiayu Zhang, Yongzhi Cao, Hanpin Wang, and Yu Huang. MR image quality assessment via enhanced mamba: A hybrid spatial-frequency approach. In *IEEE International Conference on Bioinformatics and Biomedicine, BIBM 2024, Lisbon, Portugal, December 3-6, 2024*, pages 3561–3564. IEEE, 2024. 3
- [28] Yiwei Lou, Jiayu Zhang, Dexuan Xu, Yongzhi Cao, Hanpin Wang, and Yu Huang. No-reference MRI quality assessment via contrastive representation: Spatial and frequency domain perspectives. In *IEEE International Conference on Multimedia and Expo, ICME 2024, Niagara Falls, ON, Canada, July 15-19, 2024*, pages 1–6. IEEE, 2024. 3
- [29] Shilin Lu, Yanzhu Liu, and Adams Wai-Kin Kong. TF-ICON: diffusion-based training-free cross-domain image composition. In *IEEE/CVF International Conference on Computer Vision, ICCV 2023, Paris, France, October 1-6, 2023*, pages 2294–2305. IEEE, 2023. 1
- [30] Shilin Lu, Zilan Wang, Leyang Li, Yanzhu Liu, and Adams Wai-Kin Kong. MACE: mass concept erasure in diffusion models. In *IEEE/CVF Conference on Computer Vision and Pattern Recognition, CVPR 2024, Seattle, WA, USA, June 16-22, 2024*, pages 6430–6440. IEEE, 2024. 1
- [31] Shilin Lu, Zihan Zhou, Jiayou Lu, Yuanzhi Zhu, and Adams Wai-Kin Kong. Robust watermarking using generative priors against image editing: From benchmarking to advances. *CoRR*, abs/2410.18775, 2024. 3
- [32] Xiaoqian Lv, Shengping Zhang, Chenyang Wang, Yichen Zheng, Bineng Zhong, Chongyi Li, and Liqiang Nie. Fourier priors-guided diffusion for zero-shot joint low-light enhancement and deblurring. In *Proceedings of the IEEE/CVF Conference on Computer Vision and Pattern Recognition*, pages 25378–25388, 2024.
- [33] Xintian Mao, Yiming Liu, Fengze Liu, Qingli Li, Wei Shen, and Yan Wang. Intriguing findings of frequency selection for image deblurring. In *Proceedings of the AAAI Conference on Artificial Intelligence*, pages 1905–1913, 2023. 3
- [34] Xintian Mao, Jiansheng Wang, Xingran Xie, Qingli Li, and Yan Wang. Loformer: Local frequency transformer for image deblurring. In *Proceedings of the 32nd ACM International Conference on Multimedia*, pages 10382–10391, 2024. 3
- [35] Chu-Jie Qin, Rui-Qi Wu, Zikun Liu, Xin Lin, Chun-Le Guo, Hyun Hee Park, and Chongyi Li. Restore anything with masks: Leveraging mask image modeling for blind all-in-one image restoration. *arXiv preprint arXiv:2409.19403*, 2024. 1
- [36] Zequn Qin, Pengyi Zhang, Fei Wu, and Xi Li. Fcanet: Frequency channel attention networks. In *Proceedings of the IEEE/CVF international conference on computer vision*, pages 783–792, 2021. 3
- [37] Huiyang Shao, Qianqian Xu, Peisong Wen, Peifeng Gao, Zhiyong Yang, and Qingming Huang. Building bridge across the time: Disruption and restoration of murals in the wild. In *IEEE/CVF International Conference on Computer Vision, ICCV 2023, Paris, France, October 1-6, 2023*, pages 20202–20212. IEEE, 2023. 1
- [38] Yuda Song, Zhuqing He, Hui Qian, and Xin Du. Vision transformers for single image dehazing. *IEEE Transactions on Image Processing*, 32:1927–1941, 2023. 7
- [39] Haopeng Sun. Ultra-high resolution segmentation via boundary-enhanced patch-merging transformer. *arXiv preprint arXiv:2412.10181*, 2024. 1
- [40] Haopeng Sun, Lumin Xu, Sheng Jin, Ping Luo, Chen Qian, and Wentao Liu. Program: Prototype graph model based pseudo-label learning for test-time adaptation. In *The Twelfth International Conference on Learning Representations*, 2024. 1
- [41] Shangquan Sun, Wenqi Ren, Xinwei Gao, Rui Wang, and Xiaochun Cao. Restoring images in adverse weather conditions via histogram transformer. In *Computer Vision - ECCV 2024 - 18th European Conference, Milan, Italy, September 29-October 4, 2024, Proceedings, Part XXII*, pages 111–129. Springer, 2024. 1
- [42] Roman Suvorov, Elizaveta Logacheva, Anton Mashikhin, Anastasia Remizova, Arsenii Ashukha, Aleksei Silvestrov, Naejin Kong, Harshith Goka, Kiwoong Park, and Victor Lempitsky. Resolution-robust large mask inpainting with fourier convolutions. In *Proceedings of the IEEE/CVF winter conference on applications of computer vision*, pages 2149–2159, 2022. 3
- [43] Ying Tai, Jian Yang, Xiaoming Liu, and Chunyan Xu. Memnet: A persistent memory network for image restoration. In *Proceedings of the IEEE international conference on computer vision*, pages 4539–4547, 2017. 1
- [44] Yuan Tian, Yichao Yan, Guangtao Zhai, Guodong Guo, and Zhiyong Gao. EAN: event adaptive network for enhanced action recognition. *Int. J. Comput. Vis.*, 130(10):2453–2471, 2022. 1
- [45] Yuan Tian, Guo Lu, Guangtao Zhai, and Zhiyong Gao. Non-semantics suppressed mask learning for unsupervised video semantic compression. In *IEEE/CVF International Conference on Computer Vision, ICCV 2023, Paris, France, October 1-6, 2023*, pages 13564–13576. IEEE, 2023.
- [46] Yuan Tian, Yichao Yan, Guangtao Zhai, Li Chen, and Zhiyong Gao. CLSA: A contrastive learning framework with selective aggregation for video rescaling. *IEEE Trans. Image Process.*, 32:1300–1314, 2023.
- [47] Yuan Tian, Guo Lu, Yichao Yan, Guangtao Zhai, Li Chen, and Zhiyong Gao. A coding framework and benchmark towards low-bitrate video understanding. *IEEE Trans. Pattern Anal. Mach. Intell.*, 46(8):5852–5872, 2024. 1
- [48] Fu-Jen Tsai, Yan-Tsung Peng, Yen-Yu Lin, Chung-Chi Tsai, and Chia-Wen Lin. Stripformer: Strip transformer for fast image deblurring. In *European conference on computer vision*, pages 146–162. Springer, 2022. 7
- [49] Cong Wang, Jinshan Pan, Wei Wang, Gang Fu, Siyuan Liang, Mengzhu Wang, Xiao-Ming Wu, and Jun Liu. Correlation matching transformation transformers for uhd image restoration. In *Proceedings of the AAAI Conference on Artificial Intelligence*, pages 5336–5344, 2024. 1, 3, 6, 7
- [50] Hong Wang, Qi Xie, Qian Zhao, and Deyu Meng. A model-driven deep neural network for single image rain removal. In *Proceedings of the IEEE/CVF conference on computer vision and pattern recognition*, pages 3103–3112, 2020. 6, 7

- [51] Songping Wang, Hanqing Liu, and Haochen Zhao. Public-domain locator for boosting attack transferability on videos. In *2024 IEEE International Conference on Multimedia and Expo (ICME)*, pages 1–6. IEEE, 2024. 1
- [52] Tao Wang, Kaihao Zhang, Tianrun Shen, Wenhan Luo, Bjorn Stenger, and Tong Lu. Ultra-high-definition low-light image enhancement: A benchmark and transformer-based method. In *Proceedings of the AAAI Conference on Artificial Intelligence*, pages 2654–2662, 2023. 1, 3, 6
- [53] Tao Wang, Kaihao Zhang, Ziqian Shao, Wenhan Luo, Björn Stenger, Tong Lu, Tae-Kyun Kim, Wei Liu, and Hongdong Li. Gridformer: Residual dense transformer with grid structure for image restoration in adverse weather conditions. *Int. J. Comput. Vis.*, 132(10):4541–4563, 2024. 1
- [54] Yabiao Wang, Shuo Wang, Jiangning Zhang, Ke Fan, Jiafu Wu, Zhengkai Jiang, and Yong Liu. Temporal and interactive modeling for efficient human-human motion generation. *CoRR*, abs/2408.17135, 2024. 1
- [55] Zhou Wang, Alan C Bovik, Hamid R Sheikh, and Eero P Simoncelli. Image quality assessment: from error visibility to structural similarity. *IEEE transactions on image processing*, 13(4):600–612, 2004. 6
- [56] Zhendong Wang, Xiaodong Cun, Jianmin Bao, Wengang Zhou, Jianzhuang Liu, and Houqiang Li. Uformer: A general u-shaped transformer for image restoration. In *Proceedings of the IEEE/CVF conference on computer vision and pattern recognition*, pages 17683–17693, 2022. 6, 7
- [57] Xingxing Wei, Songping Wang, and Huanqian Yan. Efficient robustness assessment via adversarial spatial-temporal focus on videos. *IEEE Transactions on Pattern Analysis and Machine Intelligence*, 45(9):10898–10912, 2023. 3
- [58] Jie Xiao, Xueyang Fu, Aiping Liu, Feng Wu, and Zheng-Jun Zha. Image de-raining transformer. *IEEE Transactions on Pattern Analysis and Machine Intelligence*, 45(11):12978–12995, 2022. 6, 7
- [59] Jie Xiao, Xueyang Fu, Yurui Zhu, Dong Li, Jie Huang, Kai Zhu, and Zheng-Jun Zha. Homoformer: Homogenized transformer for image shadow removal. In *IEEE/CVF Conference on Computer Vision and Pattern Recognition, CVPR 2024, Seattle, WA, USA, June 16-22, 2024*, pages 25617–25626. IEEE, 2024. 1
- [60] Zeyu Xiao, Zhihe Lu, and Xinchao Wang. P-bic: Ultra-high-definition image moiré patterns removal via patch bilateral compensation. In *Proceedings of the 32nd ACM International Conference on Multimedia, MM 2024, Melbourne, VIC, Australia, 28 October 2024 - 1 November 2024*, pages 8365–8373. ACM, 2024. 1
- [61] Rui Xie, Ying Tai, Kai Zhang, Zhenyu Zhang, Jun Zhou, and Jian Yang. Addr: Accelerating diffusion-based blind super-resolution with adversarial diffusion distillation. *CoRR*, abs/2404.01717, 2024. 1
- [62] Xiaogang Xu, Ruixing Wang, Chi-Wing Fu, and Jiaya Jia. Snr-aware low-light image enhancement. In *Proceedings of the IEEE/CVF conference on computer vision and pattern recognition*, pages 17714–17724, 2022. 6
- [63] Wenhan Yang, Robby T Tan, Jiashi Feng, Zongming Guo, Shuicheng Yan, and Jiaying Liu. Joint rain detection and removal from a single image with contextualized deep networks. *IEEE transactions on pattern analysis and machine intelligence*, 42(6):1377–1393, 2019. 6, 7
- [64] Xingyi Yang and Xinchao Wang. Kolmogorov-arnold transformer. *arXiv preprint arXiv:2409.10594*, 2024. 5
- [65] Tian Ye, Sixiang Chen, Wenhao Chai, Zhaohu Xing, Jing Qin, Ge Lin, and Lei Zhu. Learning diffusion texture priors for image restoration. In *Proceedings of the IEEE/CVF Conference on Computer Vision and Pattern Recognition*, pages 2524–2534, 2024. 1
- [66] Qiaosi Yi, Juncheng Li, Qinyan Dai, Faming Fang, Guixu Zhang, and Tiejong Zeng. Structure-preserving deraining with residue channel prior guidance. In *Proceedings of the IEEE/CVF international conference on computer vision*, pages 4238–4247, 2021. 6, 7
- [67] Wei Yu, Qi Zhu, Naishan Zheng, Jie Huang, Man Zhou, and Feng Zhao. Learning non-uniform-sampling for ultra-high-definition image enhancement. In *Proceedings of the 31st ACM International Conference on Multimedia, MM 2023, Ottawa, ON, Canada, 29 October 2023- 3 November 2023*, pages 1412–1421. ACM, 2023. 1
- [68] Wei Yu, Jie Huang, Bing Li, Kaiwen Zheng, Qi Zhu, Man Zhou, and Feng Zhao. Empowering resampling operation for ultra-high-definition image enhancement with model-aware guidance. In *Proceedings of the IEEE/CVF Conference on Computer Vision and Pattern Recognition*, pages 25722–25731, 2024. 1, 3
- [69] Xin Yu, Peng Dai, Wenbo Li, Lan Ma, Jiajun Shen, Jia Li, and Xiaojuan Qi. Towards efficient and scale-robust ultra-high-definition image demoiréing. In *European Conference on Computer Vision*, pages 646–662. Springer, 2022. 1, 3
- [70] Syed Waqas Zamir, Aditya Arora, Salman Khan, Munawar Hayat, Fahad Shahbaz Khan, and Ming-Hsuan Yang. Restormer: Efficient transformer for high-resolution image restoration. In *Proceedings of the IEEE/CVF conference on computer vision and pattern recognition*, pages 5728–5739, 2022. 1, 6, 7
- [71] Jiale Zhang, Yulun Zhang, Jinjin Gu, Jiahua Dong, Linghe Kong, and Xiaokang Yang. Xformer: Hybrid x-shaped transformer for image denoising. In *The Twelfth International Conference on Learning Representations*, 2024. 1
- [72] Kai Zhang, Wangmeng Zuo, Shuhang Gu, and Lei Zhang. Learning deep cnn denoiser prior for image restoration. In *Proceedings of the IEEE conference on computer vision and pattern recognition*, pages 3929–3938, 2017. 1
- [73] Li Zhang, Zean Han, Yan Zhong, Qiaojun Yu, Xingyu Wu, et al. Vocapter: Voting-based pose tracking for category-level articulated object via inter-frame priors. In *ACM Multimedia 2024*, 2024. 1
- [74] Li Zhang, Mingliang Xu, Dong Li, Jianming Du, and Ru-jing Wang. Catmullrom splines-based regression for image forgery localization. In *Proceedings of the AAAI Conference on Artificial Intelligence*, pages 7196–7204, 2024.
- [75] Li Zhang, Yan Zhong, Jianan Wang, Zhe Min, Liu Liu, et al. Rethinking 3d convolution in ℓ_p -norm space. In *The Thirty-eighth Annual Conference on Neural Information Processing Systems*, 2024.

- [76] Li Zhang, Weiqing Meng, Yan Zhong, Bin Kong, Mingliang Xu, Jianming Du, Xue Wang, Rujing Wang, and Liu Liu. U-cope: Taking a further step to universal 9d category-level object pose estimation. In *European Conference on Computer Vision*, pages 254–270. Springer, 2025. 1
- [77] Quan Zhang, Xiaoyu Liu, Wei Li, Hanting Chen, Junchao Liu, Jie Hu, Zhiwei Xiong, Chun Yuan, and Yunhe Wang. Distilling semantic priors from sam to efficient image restoration models. In *Proceedings of the IEEE/CVF Conference on Computer Vision and Pattern Recognition*, pages 25409–25419, 2024. 1
- [78] Richard Zhang, Phillip Isola, Alexei A Efros, Eli Shechtman, and Oliver Wang. The unreasonable effectiveness of deep features as a perceptual metric. In *Proceedings of the IEEE conference on computer vision and pattern recognition*, pages 586–595, 2018. 6
- [79] Yulun Zhang, Kunpeng Li, Kai Li, Bineng Zhong, and Yun Fu. Residual non-local attention networks for image restoration. *arXiv preprint arXiv:1903.10082*, 2019. 1
- [80] Chen Zhao, Weiling Cai, Chenyu Dong, and Chengwei Hu. Wavelet-based fourier information interaction with frequency diffusion adjustment for underwater image restoration. In *Proceedings of the IEEE/CVF Conference on Computer Vision and Pattern Recognition*, pages 8281–8291, 2024. 3
- [81] Chen Zhao, Weiling Cai, Chenyu Dong, and Ziqi Zeng. Toward sufficient spatial-frequency interaction for gradient-aware underwater image enhancement. In *ICASSP 2024-2024 IEEE International Conference on Acoustics, Speech and Signal Processing (ICASSP)*, pages 3220–3224. IEEE, 2024. 3
- [82] Chen Zhao, Weiling Cai, Chengwei Hu, and Zheng Yuan. Cycle contrastive adversarial learning with structural consistency for unsupervised high-quality image deraining transformer. *Neural Networks*, 178:106428, 2024. 1
- [83] Chen Zhao, Wei-Ling Cai, and Zheng Yuan. Spectral normalization and dual contrastive regularization for image-to-image translation. *The Visual Computer*, pages 1–12, 2024. 3
- [84] Chen Zhao, Chenyu Dong, and Weiling Cai. Learning A physical-aware diffusion model based on transformer for underwater image enhancement. *CoRR*, abs/2403.01497, 2024. 1
- [85] Lin Zhao, Shao-Ping Lu, Tao Chen, Zhenglu Yang, and Ariel Shamir. Deep symmetric network for underexposed image enhancement with recurrent attentional learning. In *Proceedings of the IEEE/CVF international conference on computer vision*, pages 12075–12084, 2021. 6
- [86] Zhuoran Zheng, Wenqi Ren, Xiaochun Cao, Xiaobin Hu, Tao Wang, Fenglong Song, and Xiuyi Jia. Ultra-high-definition image dehazing via multi-guided bilateral learning. In *2021 IEEE/CVF Conference on Computer Vision and Pattern Recognition (CVPR)*, pages 16180–16189. IEEE, 2021. 1, 3, 7
- [87] Zhuoran Zheng, Wenqi Ren, Xiaochun Cao, Tao Wang, and Xiuyi Jia. Ultra-high-definition image hdr reconstruction via collaborative bilateral learning. In *Proceedings of the IEEE/CVF international conference on computer vision*, pages 4449–4458, 2021. 3
- [88] Dewei Zhou, Zongxin Yang, and Yi Yang. Pyramid diffusion models for low-light image enhancement. *arXiv preprint arXiv:2305.10028*, 2023. 1
- [89] Dewei Zhou, You Li, Fan Ma, Xiaoting Zhang, and Yi Yang. MIGC: multi-instance generation controller for text-to-image synthesis. In *IEEE/CVF Conference on Computer Vision and Pattern Recognition, CVPR 2024, Seattle, WA, USA, June 16-22, 2024*, pages 6818–6828. IEEE, 2024. 1
- [90] Dewei Zhou, Ji Xie, Zongxin Yang, and Yi Yang. 3dis: Depth-driven decoupled instance synthesis for text-to-image generation. *CoRR*, abs/2410.12669, 2024. 3
- [91] Dewei Zhou, You Li, Fan Ma, Zongxin Yang, and Yi Yang. MIGC+: advanced multi-instance generation controller for image synthesis. *IEEE Trans. Pattern Anal. Mach. Intell.*, 47(3):1714–1728, 2025. 1
- [92] Man Zhou, Jie Huang, Chun-Le Guo, and Chongyi Li. Fourmer: An efficient global modeling paradigm for image restoration. In *International conference on machine learning*, pages 42589–42601. PMLR, 2023. 3
- [93] Man Zhou, Jie Huang, Keyu Yan, Danfeng Hong, Xiuping Jia, Jocelyn Chanussot, and Chongyi Li. A general spatial-frequency learning framework for multimodal image fusion. *IEEE Transactions on Pattern Analysis and Machine Intelligence*, 2024. 3
- [94] Shihao Zhou, Duosheng Chen, Jinshan Pan, Jinglei Shi, and Jufeng Yang. Adapt or perish: Adaptive sparse transformer with attentive feature refinement for image restoration. In *Proceedings of the IEEE/CVF Conference on Computer Vision and Pattern Recognition*, pages 2952–2963, 2024. 1
- [95] Wenbin Zou, Hongxia Gao, Weipeng Yang, and Tongtong Liu. Wave-mamba: Wavelet state space model for ultra-high-definition low-light image enhancement. In *Proceedings of the 32nd ACM International Conference on Multimedia*, pages 1534–1543, 2024. 1, 3, 6